First-principles study of CO and OH adsorption on in-doped ZnO surfaces

First-principles study of CO and OH adsorption on In-doped ZnO surfaces

R. Saniz[a], N. Sarmadian[a], B. Partoens[a], M. Batuk[b], J. Hadermann[b], A. Marikutsa[c], M. Rumyantseva[c], A. Gaskov[c], D. Lamoen[b]

[a] *CMT, Departement Fysica, Universiteit Antwerpen, Groenenborgerlaan 171, B-2020 Antwerpen, Belgium*
[b] *EMAT, Departement Fysica, Universiteit Antwerpen, Groenenborgerlaan 171, B-2020 Antwerpen, Belgium*
[c] *Chemistry Department, Moscow State University, Vorobyevy gory 1-3, Moscow 119991, Russian Federation*

Abstract

We present a first-principles computational study of CO and OH adsorption on non-polar ZnO $(10\bar{1}0)$ surfaces doped with indium. The calculations were performed using a model ZnO slab. The position of the In dopants was varied from deep bulk-like layers to the surface layers. It was established that the preferential location of the In atoms is at the surface by examining the dependence of the defect formation energy as well as the surface energy on In location. The adsorption sites on the surface of ZnO and the energy of adsorption of CO molecules and OH-species were determined in connection to In doping. It was found that OH has higher bonding energy to the surface than CO. The presence of In atoms at the surface of ZnO is favorable for CO adsorption, resulting in an elongation of the C-O bond and in charge transfer to the surface. The effect of CO and OH adsorption on the electronic and conduction properties of surfaces was assessed. We conclude that In-doped ZnO surfaces should present a higher electronic response upon adsorption of CO.

Keywords: Zinc oxide; doping; surfaces; first-principles methods; gas sensor; carbon monoxide

1. Introduction

Zinc oxide is a *n*-type, wide-band gap (3.2 eV) semiconductor that has long been of interest for resistive gas sensors, as well as for a range of other applications, such as in chemical production, catalysis, photocatalysis, pharmaceutics, etc. [1, 2, 3, 4, 5]. Functioning of such sensors is based on the modification of electrical properties of the semiconductor by the adsorption of gas molecules at the surface. Of particular interest are nanostructured materials with high surface-to-volume ratio, thus having enhanced gas sensitivity [5, 6, 7, 8]. However, nanocrystalline pristine ZnO has poor electronic conduction because of intrinsically low charge carrier concentration and restrictions due to the dimensions of the particles [4, 5]. A common approach to modify its electronic conduction is *n*-doping by group III metals, i.e., Al, Ga, and In [4, 7, 9, 10]. Due to the substantial discrepancy of ionic radii, the applicability of Al(III) for substitution of Zn(II) is limited [5]. Indeed, the effect of aluminum on the sensitivity of Al-doped ZnO to CO and volatile organic compounds was observed to be minor [11, 12]. This can be rationalized by the high solubility of the small Al(III) cations in bulk ZnO and the hindering of their migration to the surface. Instead, doping by Ga(III) and In(III), that have a ionic radii closer to that of Zn(II), is more often in use [4, 5]. It was demonstrated that doping ZnO with Ga improved not only the conductivity, but also the sensitivity to various toxic or flammable gases, e.g., CO, formaldehyde, H_2, ammonia, and methane [10, 13, 14, 15, 16, 17]. The influence of doping on sensitivity is often attributed to electronic effects at the semiconductor surface [13, 10], while the chemical aspect of gas molecules reception on the doped ZnO surface is overlooked. In order to tailor the functional properties of doped ZnO-based sensors, it is important to understand the effect of the dopants on the interaction between the surface and adsorbed target gas molecules. In a recent work, we demonstrated correlations between the sensitivity to H_2S and NO_2 and the surface acidity and the paramagnetic donor sites controlled by dopant content in ZnO(Ga) [18]. First-principles computational modelling based on density-functional theory (DFT) provide an efficient tool for the investigation of gas-solid interactions. For instance, the effect of dopant on CO adsorption energy and preferred adsorption position was evaluated for model ZnO(Ga) clusters [19]. Of chief interest from the modelling point of view are the preferred impurity atoms position, defect formation energies, charge transfer between adsorbed molecules and sensor surface, and the change in the surface charge carrier density upon adsorption [19, 20]. We recently initiated a joint experimental and theoretical investigation of the effect of In doping of nanocrystalline ZnO on the material structure, the interaction with CO gas and OH molecules, and the sensing behavior. CO is one of the most common and hazardous reductive air contaminants, while OH-groups are present at the oxide surface due to chemisorption of water from ambient humidity and may interfere with the sensitivity to CO target molecules. Here we present the results of a first-principles study of a model ZnO slab exposing the non-polar $(10\bar{1}0)$ surface, which is known to be the most stable and abundant ZnO surface [21]. It is, thus, the most relevant for adsorption studies.

Section II presents the methods used. Section III presents main results. In Section IV we analyze the effects of CO/OH adsorption on the electronic properties of the surfaces studies and their bearing on CO sensing. Section V is devoted to conclusions and an outlook on future work.

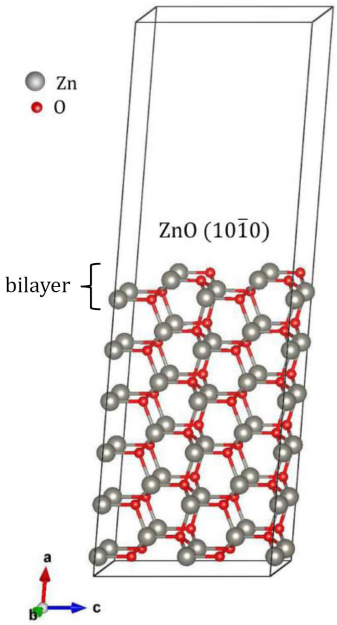

Figure 1: The $6 \times 2 \times 2$ supercell slab model used for surface calculations. The slab consists of 6 bilayers. Each layer within a bilayer comprises four Zn-O pairs. There are, thus, twelve such layers in the slab. The vacuum region is 15 Å thick.

2. Methodology

All calculations were performed within density functional theory (DFT) [22, 23], using the plane-wave basis set and the projector augmented-wave method [24, 25] as implemented in the Vienna Ab initio Simulation Package (VASP)[26, 27]. We use DFT+U [28, 29] and the Perdew-Burke-Ernzerhof (PBE) exchange and correlation potential [30]. A self-consistently calculated Hubbard U parameter of 7.16 eV is applied to the Zn atoms [31]. With this value, the calculated structural properties of bulk ZnO are in good agreement with experiment. We point out that in order to verify the reliability of our approach, we peformed calculations based on the HSE hybrid functional [32] for representative cases among the systems studied in this work, corroborating our results (we come back to this in Section 4; se also the Appendix). Our calculations for all systems studied, i.e., bulk, surfaces, and free molecules, include the van der Waals interaction (vdW-DFT) using the opt86b functional [33, 34].

We use an energy cutoff of 450 eV for the plane-wave basis set. To sample the Brillouin zone of the unit cell of bulk wurtzite ZnO, we use a $8 \times 8 \times 4$ Monkhorst-Pack (MP) grid [35] making sure that the Γ point is included in the mesh. We note that atomic relaxations are made until residual forces on the atoms are less than 0.01 eV/Å and total energies are converged to within 10^{-4} eV. To study the surface properties, we use a $6\times2\times2$ supercell slab exposing the non-polar ZnO (10$\bar{1}$0) surface. In order to minimize slab-slab interactions, the supercell includes a 15 Å vacuum space above this surface, as shown in Fig. 1 [36]. The slab electronic structure is determined using a $1 \times 4 \times 4$ MP grid including the Γ point. The surface energy

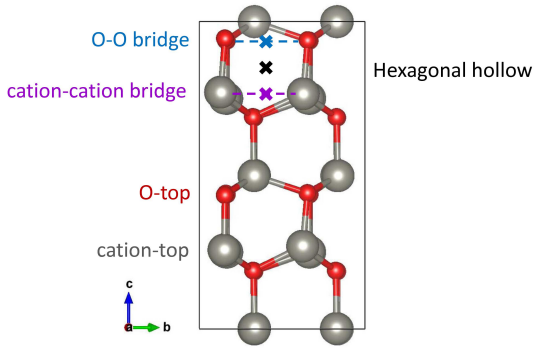

Figure 2: Top view of the slab supercell, with the possible initial adsorption locations considered here indicated (the lattice vectors in this figure are the same as in Fig. 1).

E_s (for either a pure or In-doped surface) is calculated using

$$E_s = (E_{\text{slab}} - E_{\text{supercell}})/2A \quad (1)$$

where E_{slab} and $E_{\text{supercell}}$ denote the total energies of the relaxed slab (pure or In-doped) and of a bulk supercell (pure or In-doped) with an equivalent number of formula units. A is the surface area of the slab. The slab consists of six bilayers (see Fig. 1), each consisting of two neutral Zn-O layers (this is, twelve layers in all). Previous authors have shown that with this number of layers the surface energy is converged with respect to slab thickness [21]. As seen in Fig. 1, each of these layers contains four Zn-O pairs. When relaxing the slab structure, we keep the three lowest bilayers fixed to simulate the rigidity of the bulk-like deeper subsurface layers in a real sample. We henceforth refer to the upper six Zn-O layers (corresponding to the upper three bilayers) as the six surface-like layers [37]. There are two technical issues to consider here. First, the relaxation we perform results in an asymmetric slab, giving rise to a non-constant potential in the vacuum region although the surfaces we consider are non-polar. Such a potential may affect the properties of the system studied. Further, in the case of adsorbed molecules, dipoles can be formed because of charge transfer between the surface and the latter, and dipole-dipole interactions may also have an effect. We verified that these effects are negligible, however, by comparing the electronic structure of our ZnO slab with and without dipole corrections, both for a pristine slab and for an In-doped slab with CO adsorbed (see Supplementary Material). Second, in the case of the In-doped slabs, charge carriers can be sensitive to slab thickness because of their long range response to perturbations. Thus, it is important to verify that a slab thickness of six bilayers is sufficient to minimize size effects. For this we considered again the important case of CO adsorption and performed the calculations for an eight bilayer thick slab as well. The results show that the six bilayer slab is indeed sufficient (see Supplementary Material).

Regarding doping, our experimental evidence indicates that a 4-5 at.% In concentration [i.e., [In]/([In]+[Zn])] is sufficient for it to overcome its solubility in ZnO and to segregate to the surface [38]. These experiments suggest that the sensitivity of

the surface is enhanced by the presence of dopants such as In at the surface. Thus, here we substitute two Zn atoms with In in our supercell slab model, which represents an In concentration of 4.17 at.%. The impurity, or dopant, formation energy in a neutral charge state (either in the bulk or slab systems) is given by [39]

$$E_f = E_{\text{doped}} - E_{\text{pure}} - n\mu_{\text{In}} + n\mu_{\text{Zn}}, \quad (2)$$

where E_{doped} is the total energy of the system containing the dopants and E_{pure} is the total energy of pure system (undoped slab or bulk ZnO) [40]. μ_{In} and μ_{Zn} are the chemical potentials of In and Zn, respectively, and n is the number of Zn atoms substituted. The chemical potentials are calculated in their ground state metallic phases, i.e., tetragonal for In and hexagonal close-packed for ZnO. When studying the effects of the location of the dopants with respect to the topmost surface, the two In atoms substitute two Zn atoms in a single surface-like layer at a time. The two substitution sites in a layer are determined by minimizing the total energy. We denote S_i ($i = 1, \ldots, 6$) the slab with the In atoms sitting in its i-th surface-like layer (S_1 being the case where the In atoms are in the topmost layer).

In order to study the adsorption of CO or OH, we place one such a molecule on top of the relaxed ZnO slab, at a distance of 2 Å from the surface. We consider six possible initial positions, namely cation-top (in the case of a doped surface the cation can be Zn or In), O-top, center of hexagonal hollow, cation-cation-bridge, and O-O-bridge. The possible adsorption sites are shown in Fig. 2. The positions of the CO/OH molecule and of atoms in the surface-like layers of the slab are optimized. The adsorption energy E_a of the adsorbed molecule is defined as

$$E_a = E_{\text{CO/OH–ZnO}} - E_{\text{CO/OH}} - E_{\text{ZnO}}, \quad (3)$$

where $E_{\text{CO/OH–ZnO}}$ denotes the total energy of the slab with the adsorbed molecule, and $E_{\text{CO/OH}}$ and E_{ZnO} denote the total energies of the free CO/OH molecule and of the ZnO slab, respectively. Note that the adsorption of one CO/OH molecule on top of a (2×2) surface is equivalent to 1/4 monolayer (ML) molecular coverage.

In addition, in order to understand the adsorption process and the contribution of different atoms in this process, we analyze the atomic species character of the energy bands (levels) close to the Fermi level and band edges of the ZnO surfaces, with and without CO/OH molecule adsorption. Finally, the calculated electron charge density of the optimized structure is used to calculate the electronic charge partitioned for each atom using a grid-based Bader charge analysis [41, 42]. Charge transfer between an absorbed molecule and a surface can be determined using

$$\Delta q = -e\Delta n = -e(n_{\text{atom}} - n_{\text{valence}}), \quad (4)$$

where n_{atom} is the calculated number of electrons around an atom in the system studied and n_{valence} is the number of valence electrons considered for the calculations for the corresponding atom. This is used to further characterize the adsorption process.

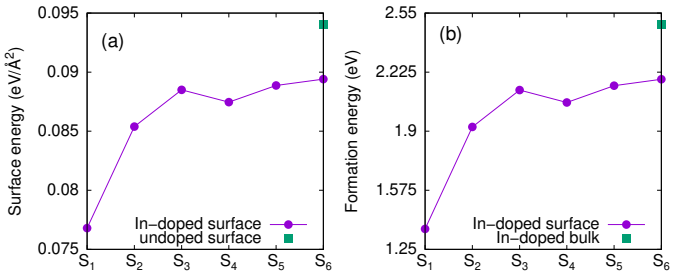

Figure 3: (a) Surface energy of the In-doped ZnO S_i slabs, in comparison with the surface energy of the undoped ZnO surface. (b) Formation energy of the In impurities in the S_i slabs, compared with the formation energy of bulk In-doped ZnO.

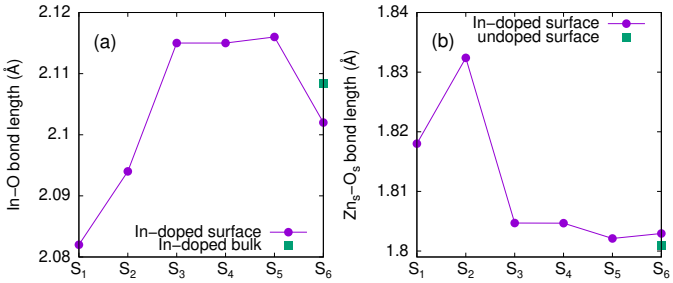

Figure 4: Structural change of the ZnO surfaces with In doping. (a) Length (average) of the In-O bond and (b) of the surface Zn to surface O bonds (Zn_s-O_s). The corresponding bulk bond lengths are shown for comparison in both plots.

3. Results

3.1. In-doped ZnO surfaces

We consider first the effect of doping on the surface energy. For the undoped surface we find an energy of 0.094 eV/Å^2. This can be compared with the value of 0.081 eV/Å^2 obtained in Ref. 21 using the B3LYP hybrid-functional. In Fig. 3(a) we plot the surface energies of the In-doped slabs as a function of location of the dopants, comparing them with the energy of the undoped surface. As expected from the observation of In segregation to the surface in experiment [38], the surface energy tends to decrease as the In dopants approach the slab surface, reaching its lowest value (0.077eV/Å^2) at S_1. The trend is mirrored by the dopant formation energies, shown in Fig. 3(b), where E_f per In atom is plotted. This shows more directly that the In impurities will tend to segregate to the surface.

We also study the surface structural changes induced by doping. Figure 4(a) shows the average In-O bond length in the S_i slabs (as noted above, there are two In-O pairs in each case), compared to the corresponding bond length in a In-doped bulk supercell. Further, we consider the average bond length of the Zn-O pairs at the *surface* of the slab, which we denote Zn_s-O_s. In Fig. 4(b) we show how that bond length depends on how far from the surface the In dopants lie, and compares it with the same bond length in the undoped surface. Figures 4 indicate that the structural changes are more pronounced when the In dopants lie at the surface or subsurface of the slabs. Since these cases also present the lowest formation energies (Figs. 3), we

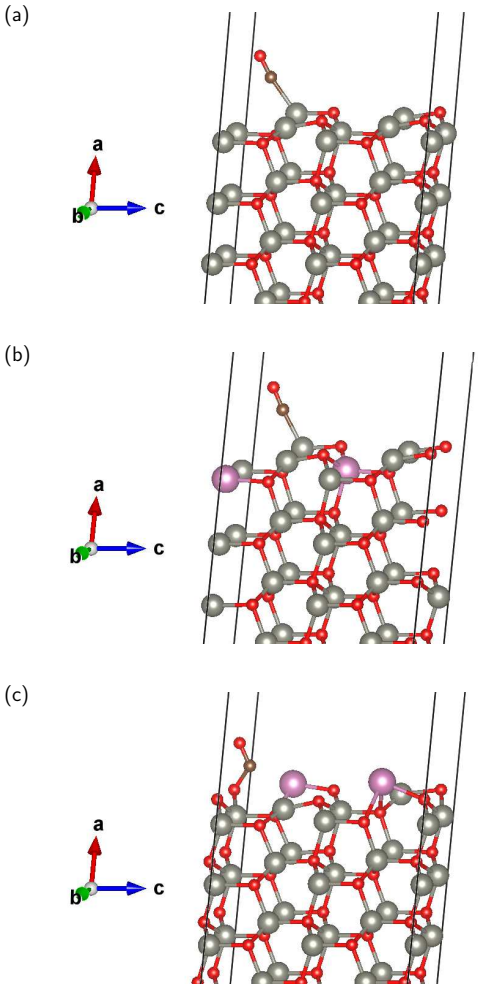

Figure 5: Structure of the relaxed CO molecule-ZnO surface systems, for the cases of (a) the undoped surface, (b) the S_2 slab, and (c) the S_1 slab. The carbon and indium atoms are represented by the brown and magenta spheres, respectively. In the first two cases CO is essentially physisorbed, with the depicted bond being very weak (see text). In (c) the CO molecule is chemically bond to a surface oxygen, away from the In dopants.

focus on these cases in our study below on molecule adsorption.

3.2. CO/OH adsorption

We study the adsorption of CO and OH on undoped surfaces as well as on the In-doped surfaces S_1 and S_2, as indicated above. In each case we determined the preferred adsorption site via the comparison of the total energies corresponding to the different sites indicated in the previous Section (see Fig. 2). Here we look more closely into the characteristics of the preferred sites.

We consider first CO adsorption. The relaxed structures in the three cases above indicated are shown in Fig. 5. In the case of the undoped surface [Fig. 5(a)], the CO molecule relaxes to the center of the hexagonal hollow. Note that because the CO molecule does not stand vertically above the surface, the C atom is closer to one of the Zn atoms forming the hexagonal hollow, and appears bonded to it. In the S_2 case the CO molecule relaxes more clearly to a Zn-top position, and bonds with the Zn atom (the bond length is smaller than in the previous case; see further down). In the S_1 case, the CO molecule relaxes to an O-top positions. More exactly, it relaxes to what we call a O_{Zn} position. Indeed, in the S_1 case, two different O-top adsorption positions are possible: one is above of the O atom in the In-O pair (O_{In}), and the other above the O atom in the Zn-O pair (O_{Zn}). The relaxed surface structure in the S_1 case is shown in Fig. 5(c). Note that the possible reaction of CO on metal oxides surfaces with pre-adsorbed or lattice oxygen has been studied many times in the past [43]. Such a mechanism has been invoked, for instance, in the study of the CO sensing properties of Ti-doped SnO surfaces [44]. Furthermore, the possible reaction of CO with adsorbed oxygen has been hypothesized by the group of G. Neri in a series of experimental articles studying the CO sensing properties of ZnO doped with Al, Ga, and In [7, 10, 45]. Interestingly, here we find that CO can interact with a lattice oxygen when the surface is In-doped.

In the case of OH adsorption, the results are markedly different. On the undoped surface and on S_2 the OH molecule relaxes to the Zn-Zn bridge position, although the OH molecule orientation with respect to the surface is different. This is shown in Figs. 6(a) and (b), respectively. In Fig. 6(b) the bridge cannot be seen because the OH molecule bridges Zn atoms in neighboring cells along the *b* direction, and only the atoms in a single cell are shown. In the case of S_1, the OH molecule relaxes to a Zn-In bridge position, as seen in Fig. 6(c).

We now look in more detail into how In doping affects the surface structure and how it correlates with the adsorption energy of the adsorbed molecules and with charge transfer between the latter and the surfaces. In Fig. 7(a) we consider the interatomic bond length of the CO and OH molecules themselves, where we compare the bond length of the isolated molecules with their bond length when adsorbed on an undoped surface (U), and on doped surfaces S_1 and S_2. We can see that in the case of the OH molecule, the bond length is only weakly affected by the surface, whether the latter is In-doped or not. In the case of the CO molecule, its bond legth is also weakly af-

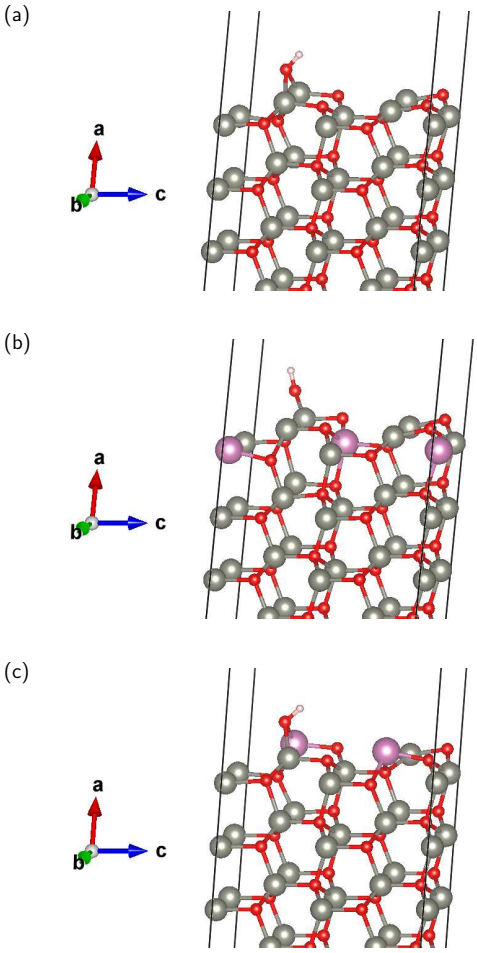

Figure 6: Structure of the relaxed OH molecule-ZnO surface systems, for the cases of (a) the undoped surface, (b) the S_2 slab, and (c) the S_1 slab. The hydrogen atom is represented by a white sphere (the indium atoms are represented by magenta spheres, as in Figs. 5). In all cases, the OH molecule is chemically bonded to the surface via a bridge bond (Zn-Zn bridge in (a) and (b), and Zn-In bridge in (c).

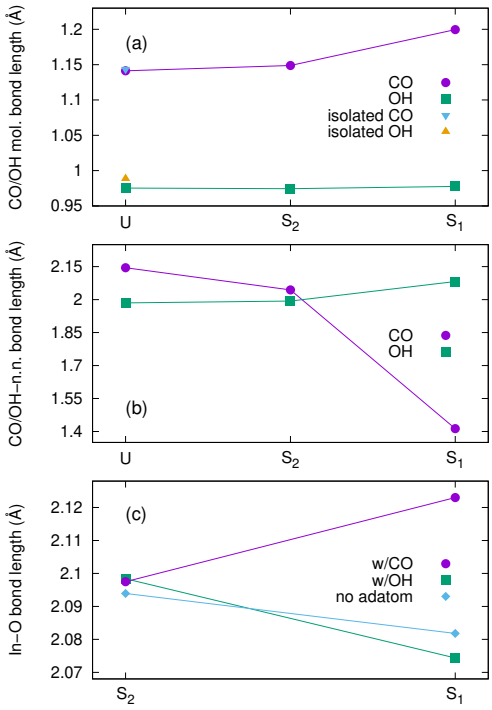

Figure 7: (a) Intramolecular bond lengths for the CO and OH molecules adsorbed on the undoped and S_1 and S_2 slabs. (b) Bond length of the CO or OH molecules to their nearest neighbor in the slabs. (c) Average In-O bond lengths in the S_1 and S_2 slabs, compared to the bond length in the case with no adsorbed molecule.

fected in the undoped surface and S_2 cases. However, in the S_1 case, the bond length is elongated by as much as 5%.

To complement this information, we consider the distance between the adsorbed molecules and the surface, i.e., the bond length between C (O) in the CO (OH) molecule and its nearest neighbor on the ZnO surface (in the case of the bridge positions, we consider the average of the bond lengths involved). These bond lengths are shown in Fig. 7(b). Again, doping affects the CO molecule considerably more than the OH molecule. In the latter case the average bridge bond length hardly changes between the undoped surface and S_2, elongating by close to 4.9% on S_1. On the other hand, in the case of the CO molecule the bond length is 4.7% shorter on S_2 than on the undoped surface. But on S_1 the bond length is dramatically shorter, falling by 34% with respect to the bond length on the undoped surface. The main reason for such a strong difference is of course that on S_1 the CO molecule is bonded to a surface oxygen, while on the undoped surface (and S_2) it is bonded to zinc. Finally, it is interesting to see the effect of the adsorbed molecules on the In-O bond lengths in the case of the doped surfaces. This is illustrated in Fig. 7(c). We can see that the adsorbed molecules have relatively little effect on the In-O bond length when In doping occurs in the subsurface (S_2). On the other hand, in the case of S_1 the adsorption of CO and OH has opposite effects. The latter decreases the bond length by less than 0.4%, while the former elongates it by nearly 2%.

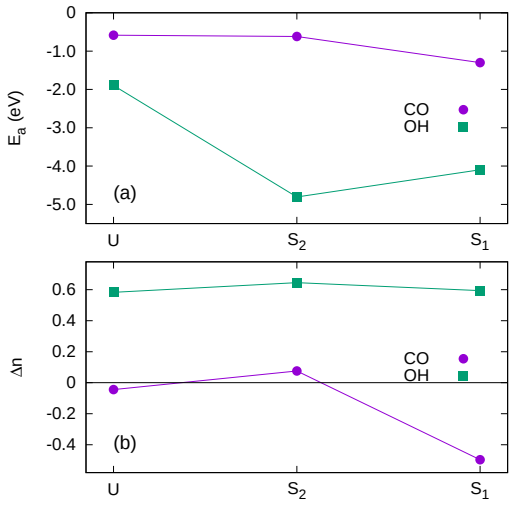

Figure 8: (a) CO and OH adsorption energies to the undoped and S_1 and S_2 slabs. (b) Molecule number of electrons gain or loss for the CO and OH molecules in the three cases indicated in (a).

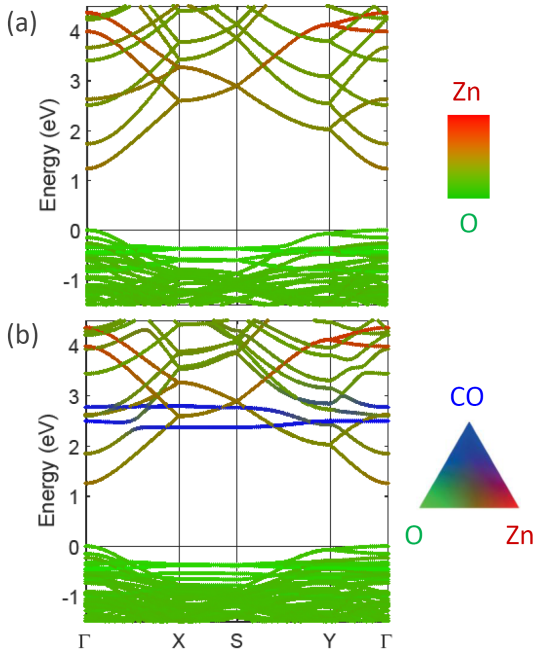

Figure 9: Character of the band structures of (a) the undoped ZnO slab, with the colors highlighting the Zn and O contributions (red and green, respectively), and (b) the undoped slab with CO adsorbed, the contribution of the latter highlighted in blue.

In Fig. 8(a) we show the adsorption energies of the CO and OH molecules on the undoped and doped surfaces. The value we obtain for CO adsorbed on the undoped surface is 0.59 eV. This is a comparatively weak value, indicative of physisorption. This is in line with experiment, where ultraviolet photoelectron spectroscopy measurements on ZnO powders yield an adsorption energy value of $\sim$ 0.52 eV (note that in such experiment, polar as well as non-polar surfaces are probed) [46]. The value increases only slightly in the case of the S_2 surface. In the case of the S_1 surface, however, the adsorption energy increases to 1.30 eV, indicating that CO is actually chemically bound to the surface. The OH adsorption energies are much stronger in all cases. Our calculated value for the undoped surface, 1.90 eV, compares well with previously reported values, 1.72 or 1.78 eV [47]. As for CO, doping the surfaces with In increases the adsorption energies.

The charge transfer between CO and OH and the ZnO surfaces yields additional information on the nature of the adsorption. Fig. 8(b) shows that there is strong charge transfer toward the OH molecule [see Eq. (4)] in all cases, consistent with a chemical bond. In contrast, the CO molecule shows only very weak charge transfer in the cases of the undoped surface and surface S_2, which is typical of physisorption. However, in the case of surface S_1 there is a much stronger charge transfer, toward the surface in this case, which is congruent with the stronger adsorption energy indicated above.

We point out here that we considered the possibility of having CO and OH adsorbed simultaneously on our surface model. We found that the formation energy in that case is between 0.08 and 0.66 eV higher than the formation energy for CO and OH adsorbed separately, depending on the surface (S_2 or S_1). Note that those energies correspond to temperatures above 900 K. Thus, we do not address that situation here.

4. Effect of adsorption on surface electronic properties and semiconductor behavior

We discuss here the implications that the adsorption of gas molecules has on the electronic properties of In-doped ZnO surfaces. For this we look into the character of the states near the valence band maximum (VBM) and conduction band minimum (CBM) of the ZnO slabs and how these are modified by the In-doping and by the adsorption of CO and OH.

In Fig. 9(a) we plot the band structure of a pure ZnO slab, i.e., with no In doping and with no adsorbed molecule [48]. The slabs present rectangular symmetry on the *bc*-plane, and the bands correspond to states along the high symmetry lines on the same plane. The zero of energy is set at the VBM. The ZnO slab remains a semiconductor, with the VBM and CBM both at the Γ point, as in bulk ZnO. The color indicates the character of the bands. Thus, the valence bands have a clearly dominant oxygen character, while the conduction bands have more mixed character, with some bands showing stronger zinc or oxygen contribution. In Fig. 9(b) we consider the effect of CO adsorption. The CO bonding molecular levels are deep, well below the minimum energy in the plot, with the antibonding levels well above the CBM and clearly very weakly hybridized with the ZnO levels. Thus, the valence and conduction bands are largely left untouched. This indicates that the CO molecule is not chemically bound to the surface, in agreement with our assessment based on bond lengths, adsorption energy, and charge transfer presented in the previous Section. Quite importantly, this means that the electronic properties of pure ZnO $(10\bar{1}0)$ surfaces would be practically unaffected by

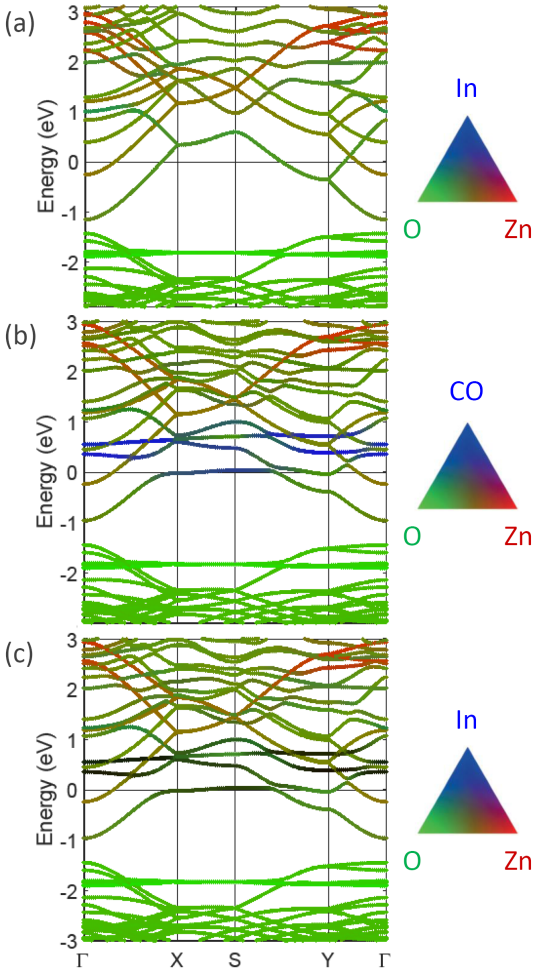

Figure 10: Character of the band structures of (a) the In-doped ZnO slab with no CO adsorbed, with the colors highlighting the In, Zn, and O contributions (blue, red, and green, respectively); (b) the S_2 slab with CO adsorbed, with the colors highlighting the CO, Zn, and O contributions (blue, red, and green, respectively); (c) same as in (b), but with blue highlighting the In contribution.

adsorbed CO molecules and, hence, that inferior CO sensitivity can be expected from undoped ZnO surfaces.

In Fig. 10 we consider the S_2 slabs. Figure 10(a) presents the band structure of a S_2 slab with no CO adsorbed. This band structure is very close to the band structure of bulk In-doped ZnO, although the band gap narrowing here is stronger (see, e.g., Ref. 49). The excess In electrons (with respect to Zn) go on to populate the lowest conduction band, thus loosing their In character and becoming delocalized. The S_2 slab, therefore, remains an *n*-type doped semiconductor, showing no great consequential surface effects from the electronic point of view. Figures 10(b) and (c) present the band structure when a CO molecule is adsorbed on the surfaces of S_2, highlighting (in addition to O and Zn) the contribution of the CO molecule [(b)] and of In [(c)]. Again the CO molecule states shows little hybridization with the surface atoms. This agrees with the weak adsorption energy and low charge transfer shown in Figs. 8(a) and (b) [note that the bond lengths in Figs. 7(a) and (b) show little change with respect to the CO molecule adsorbed on the

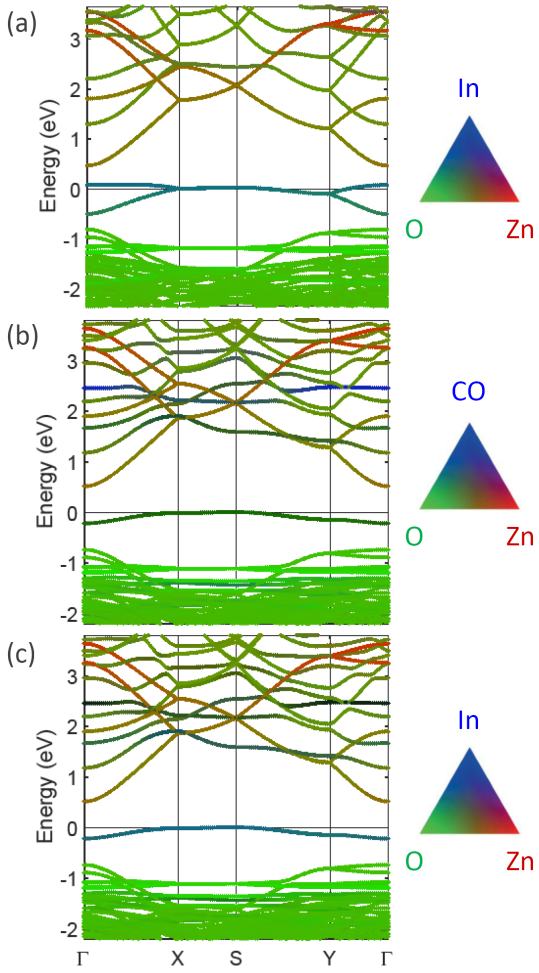

Figure 11: Same as Fig. 10, but for the case of the S_1 slab.

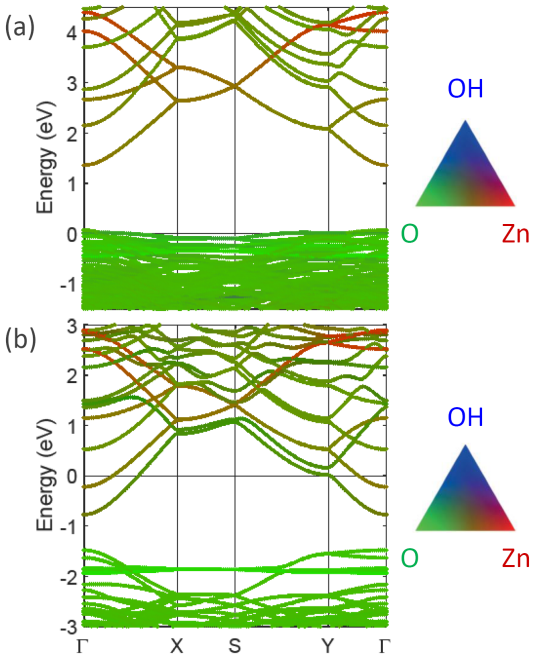

Figure 12: Character of the band structures of (a) the undoped ZnO slab with OH adsorbed, with the colors highlighting the OH, Zn, and O contributions (blue, red, and green, respectively), and (b) similar for the S_2 slab.

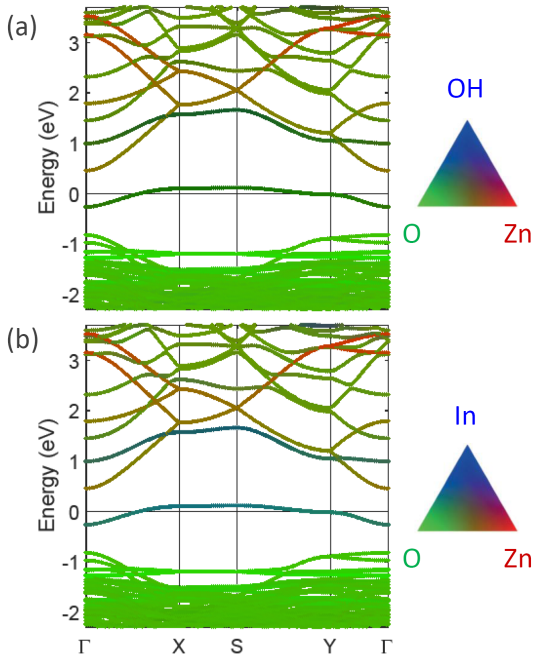

Figure 13: Character of the band structure of the S_1 slab with OH adsorbed, showing in (a) the OH, Zn, and O contributions (blue, red, and green, respectively), and in (b) the In, Zn, and O contributions, blue indicating In in this plot.

undoped ZnO surface; compare also Figs. 5(a) and (b)]. We can see in Fig. 10(b) that there are some CO states near the Fermi level along the X-S high symmetry line (the states close to S actually fall just above the Fermi level and are empty). This gives rise to the weak positive charge transfer in Fig. 8(b) in this case. The effect of these states on the electronic properties of the slab, however, are expected to be weak because of the small fraction of charge involved. Thus, we conclude that as long as the In dopants reside at the interior of the slab, they will not result in a surface electronically sensitive to CO.

Matters change significantly in the case of the S_1 slab. Figure 11(a) shows the band structure of the S_1 slab with no CO adsorbed. It clearly indicates that the In dopants create highly localized states in the band gap, arising from the In dangling bonds at the surface (the non-zero dispersion in these state in the plot is only due to the small size of the supercell, especially in the *b* direction). Thus, because of band bending at the surface, these states will act as electrons traps and hinder the *n*-type conductivity arising from any In dopants in the interior of the slab (case above). The effect of CO adsorption is significant. As Figs. 11(b) and (c) show, it results essentially in passivation of the In dangling bonds (adsorption of only one CO molecule is considered in this study), consequently eliminating the electron traps associated to them and thus increasing *n*-type conductivity of the slab. This picture is supported by a charge density difference plot showing how charge is redistributed between the CO molecule and the surface, as shown in Fig. A.15 in the Appendix. Thus, the presence of In atoms at the surface of ZnO(In) is favorable for the electronic signal generation upon CO adsorption. The processes of adsorption of target gas molecules and of oxidation of adsorbates at the sensor surface determine the sensing behavior. Hence, the sensitivity of In-doped ZnO to CO should be improved once the dopant segregates to the surface.

We now consider briefly the effects of OH adsorption. Figure 12(a) shows that on an undoped slab OH adsorption leads to empty states around the VBM. This results from the strong hybridization of the OH levels with Zn and O upper surface levels. This indicates that the OH molecule will be chemisorbed, in agreement with what was suggested by Figs. 7, 8, and 9. Thus the surface will be *p*-type, although the mobility of the holes will be low because of the high hole mass. In Fig. 12(b) we consider the S_2 slab with OH adsorbed. The plot shows that the slab will continue to be *n*-type, but with a noticeable charge carrier decrease [compare with Fig. 10(a)]. This is due to the strong charge transfer involved in the OH-Zn bridge bonds depicted in Fig. 6(b) [see also Fig. 8(b)]. In Fig. 12(b) the OH levels are deep, below the lowest energies shown. Indium does not contribute significantly in the energy range in the figure, so the corresponding plot is not shown.

In Fig. 13 we consider OH adsorbed on slab S_1. As the plots show, OH tends to passivate the In dangling bonds at the surface similar to CO. This suggests that the adsorbed OH molecules will interfere with the signals produced by CO adsorption. Thus, overall, OH would have a negative impact on the CO sensing properties of the In-doped slabs.

5. Summary and conclusions

In summary, we present a first-principles computational study of CO and OH adsorption on non-polar ZnO $(10\bar{1}0)$ surfaces doped with indium. We find that In substitutes Zn preferentially at the surface. The presence of In atoms at the surface of ZnO favors CO adsorption, resulting in an elongation of the C-O bond and in charge transfer to the surface. Our charge transfer and band structure analysis shows that CO tends to passivate the In dangling bonds when it is located at the surface. This indicates that In doping at the surface of ZnO should increase the electronic response of the latter upon adsorption of CO. On the other hand, the adsorption of OH molecules on the surfaces we studied will tend to have a negative impact on their CO sensing properties. It is important to point out, however, that further work is needed in order to have a more complete picture of the phenomenology of CO adsorption on In-doped ZnO surfaces. Indeed, the dissociative adsorption of H_2O should be considered, as this is often the source of OH groups at the surface in humid conditions. The adsorption of H, O, and O_2 should also be studied. In addition, ZnO surfaces can be expected to present native defects, which can also play an important role when it comes to CO adsorption.

Acknowledgments

We acknowledge the financial support of FWO-Vlaanderen through project G0D6515N and of the ERA.Net RUS Plus initiative through grant No. 096 (FONSENS). The computational resources and services used in this work were provided by the VSC (Flemish Supercomputer Center) and the HPC infrastructure of the University of Antwerp (CalcUA), both funded by FWO-Vlaanderen and the Flemish Government-department EWI.

Appendix A.

Appendix A.1. Comparison with HSE calculations

Electronic structures obtained within a DFT+U approach depends importantly on the U value used. It has a strong influence, for instance, on the calculated band gap value of semiconductors. Some of our main conclusions are based on the analysis of the band structure of the slabs we studied. It is important, thus, to validate the approach in this study. The HSE hybrid functional offers a method of choice for a comparison because of its reliability in determining the electronic structure of semiconductors. Unfortunately, it is computationally demanding, and cannot be applied systematically to study large systems like the present ones. Therefore, here we focus on the band structures resulting in two of the most crucial observations in our study, namely the localized states in the band gap in the case of the S_1 slab, and their passivation by CO adsorption.

In Fig. A.14 we present the HSE band structures corresponding to Figs. 11(a) and (b). The HSE calculations were perfomed using the same atomic positions, same **k**-point grid, and same computational parameters as in the DFT+U calculations. The HSE calculations were done using a 0.375 fraction of exact

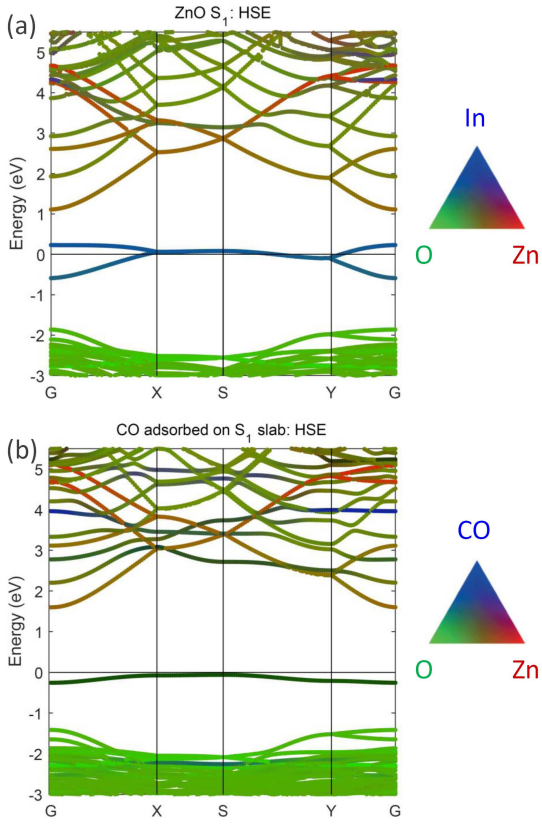

Figure A.14: Character of the band structure of the S_1 slab with CO adsorbed, showing in (a) the In, Zn, and O contributions (blue, red, and green, respectively), and in (b) the CO, Zn, and O contributions, blue indicating CO in this plot.

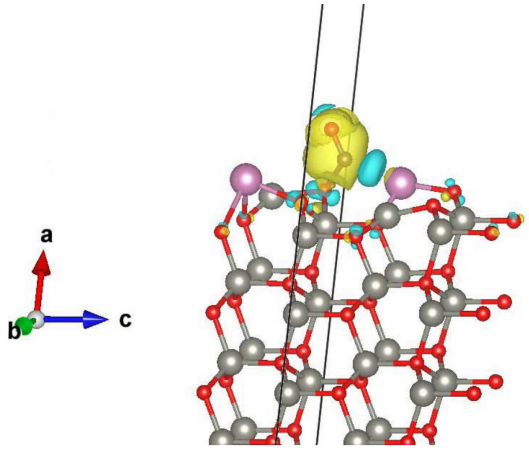

Figure A.15: Plot of the charge density difference, as defined in Eq. (A.1). In Fig. 5(c) one can see that the CO molecule sits at the extreme left side of the top surface. For clarity, in the above figure the plotting window has been shifted so that the CO molecule is at the center of the top surface.

Hartree-Fock exchange, which correctly reproduces the experimental band gap of wurtzite ZnO [50]. Fig. A.14(a) should be compared with Fig. 11(a), and Fig. A.14(b) with Fig. 11(b). The main differences are a wider gand gap in the HSE case, as one could expect, and band dispersions (band widths). However, the presence and nature of the states in the band gap in Figs. 11(a) and A.14(a) is essentially the same, being localized and of dominant In character, with some admixture of oxygen content. Moreover, the passivation of these gap states by CO adsorption, with otherwise little effect on the electronic structure, takes place in the most similar way in both calculations, as the comparison of Figs. (b) shows.

The above shows that our band structure analysis in the main text and the conclusions drawn thereupon are sound.

Appendix A.2. CO on S_1: charge density difference

In order to shed more light onto the nature of the CO bonding to the surface in the case of slab S_1, we present in Fig. A.15 below a charge density difference plot, defined as

$$\delta\rho = \rho_{\mathrm{CO\,on}\,S_1\,\mathrm{slab}} - \rho_{S_1\,\mathrm{slab}} - \rho_{\mathrm{CO\,alone}}. \qquad \text{(A.1)}$$

The charge density difference $\delta\rho$ varies between $-1.63e$ and $+0.07e$ per unit volume. The plot shows the isosurface for $|\delta\rho| = 0.0075e$ per unit volume, with yellow indicating a positive charge density and cyan a negative charge density (the isosurfaces for larger absolute values rapidly shrink around the ions, and information on bonding is lost). The plot can be readily interpreted as illustrating how CO tends to passivate the In dangling bonds, in support of our discussion on Fig. 11 and one of the main conclusions of our work.

References

References

[1] J. I. Shulin and Y. E. Changhui, Synthesis, Growth Mechanism, and Applications of Zinc Oxide Nanomaterials, J. Mater. Sci. Technol. 24 (2008) 457.

[2] A. Kołodziejczak-Radzimska and T. Jesionowski, Zinc Oxide-From Synthesis to Application: A Review, Materials 7 (2014) 2833.

[3] T. Seiyama and S. Kagawa, Study on a detector for gaseous components using semiconductive thin films, Anal. Chem. 38 (1966) 1069.

[4] K. Ellmer, Transparent Conductive Zinc Oxide and Its Derivatives, in *Handbook of Transparent Conductors*, D. S. Ginley (Ed.) (Springer, New York, 2010), p. 193.

[5] S. J. Pearton, D. P. Norton, K. Ip, Y. W. Heo, and T. Steiner, Recent progress in processing and properties of ZnO, Prog. Mat. Sci. 50 (2005) 293.

[6] Q. Wan, Q. H. Li, Y. J. Chen, T. H. Wang, Fabrication and ethanol sensing characteristics of ZnO nanowire gas sensors, X. L. He, J. P. Li, and C. L. Lin, Appl. Phys. Lett. 84 (2004) 3654.

[7] M. Hjiri, L. El Mir, S. G. Leonardi, Al-doped ZnO for highly sensitive CO gas sensors, A. Pistone, L. Mavilia, and G. Neri, Sens. Actuators B 196 (2014) 413.

[8] Y. V. Kaneti, Z. Zhang, J. Yue, Q. M. D. Zakaria, C. Chen, X. Jiang, and A. Yu, Crystal plane-dependent gas-sensing properties of zinc oxide nanostructures: experimental and theoretical studies, Phys. Chem. Chem. Phys. 16 (2014) 11471.

[9] F. Paraguay D., M. Miki-Yoshida, J. Morales, J. Solis, and L. W. Estrada, Influence of Al, In, Cu, Fe and Sn dopants on the response of thin film ZnO gas sensor to ethanol vapour, Thin Solid Films 373 (2000) 137.

[10] M. Hjiri, R. Dhahri, L. El Mir, A. Bonavita, N. Donato, S. G. Leonardi, and G. Neri, CO sensing properties of Ga-doped ZnO prepared by sol-gel route, J. Alloy. Compd. 634 (2015) 187.

[11] S. K. Lim, S. H. Hong, S.-H. Hwang, W. M. Choi, S. Kim, H. Park, and M. G. Jeong, Synthesis of Al-doped ZnO Nanorods via Microemulsion Method and Their Application as a CO Gas Sensor, J. Mater. Sci. Technol. 31 (2015) 639.

[12] C.-L. Hsu, D.-X. Hsu, T.-J. Hsueh, S.-P. Chang, and S.-J. Chang, Transparent gas sensor and photodetector based on Al doped ZnO nanowires synthesized on glass substrate, Ceram. Int. 43 (2017) 5434.

[13] Y. Hou and A. H. Jayatissa, Low resistive gallium doped nanocrystalline zinc oxide for gas sensor application via sol-gel process, Sens. Actuators B 204 (2014) 310.

[14] L. Nulhakim, H. Makinoa, S. Kishimoto, J. Nomoto, and T. Yamamoto, Enhancement of the hydrogen gas sensitivity by large distribution of c-axis preferred orientation in highly Ga-doped ZnO polycrystalline thin films, Mat. Sci. Semicon. Proc. 68 (2017) 322.

[15] D.-T. Phan and G.-S. Chung, Effects of defects in Ga-doped ZnO nanorods formed by a hydrothermal method on CO sensing properties, Sens. Actuators B 187 (2013) 191.

[16] K. Kim, Y.-W. Song, S. Chang, I.-H. Kim, S. Kim, and S. Y. Lee, Fabrication and characterization of Ga-doped ZnO nanowire gas sensor for the detection of CO, Thin Solid Films 518 (2009) 1190.

[17] N. Han, Y. Tian, X. Wu, and Y. Chen, Improving humidity selectivity in formaldehyde gas sensing by a two-sensor array made of Ga-doped ZnO, Sens. Actuators B 138 (2009) 228.

[18] N. Vorobyeva, M. Rumyantseva, D. Filatova, E. Konstantinova, D. Grishina, A. Abakumov, S. Turner, and A. Gaskov, Nanocrystalline ZnO(Ga): Paramagnetic centers, surface acidity and gas sensor properties Sens. Actuators B 182, 555 (2013).

[19] M. Derakhshandeh and H. Anaraki-Ardakani, A computational study on the experimentally observed sensitivity of Ga-doped ZnO nanocluster toward CO gas, Physica E 84 (2016) 298.

[20] M. Khuili, N. Fazouan, H. A. El Makarim, G. El Halani, and El H. Atmani, Comparative first principles study of ZnO doped with group III elements, J. Alloy. Compd. 688 (2016) 368.

[21] N. L. Marana, V. M. Longo, E. Longo, J. B. L. Martins, and J. R. Sambrano, Electronic and Structural Properties of the $(10\bar{1}0)$ and $(11\bar{2}0)$ ZnO Surfaces J. Phys. Chem. A 112 (2008) 8958.

[22] P. Hohenberg, and W. Kohn, Inhomogeneous electron gas, Phys. Rev. 136 (1964) B864.

[23] W. Kohn, and L. J. Sham, Self-consistent equations including exchange and correlation effects, Phys. Rev. 140 (1965) A1133.

[24] G. Kresse, and D. Joubert, From ultrasoft pseudopotentials to the projector augmented-wave method, Phys. Rev. B 59 (1999) 1758.

[25] P. E. Blöchl, Projector augmented-wave method, Phys. Rev. B 50 (1994) 17953.

[26] G. Kresse, and J. Hafner, Ab initio molecular dynamics for liquid met-

als, Phys. Rev. B 47 (1993) R558; Norm-conserving and ultrasoft pseudopotentials for first-row and transition-elements, J. Phys. Cond. Matt. 6 (1994) 8245.
[27] G. Kresse, and J. Furthmüller, Efficiency of ab-initio total energy calculations for metals and semiconductors using a plane-wave basis set, Comput. Mater. Sci. **6**, 15 (1996); Efficient iterative schemes for ab initio total-energy calculations using a plane-wave basis set, Phys. Rev. B 54 (1996) 11169.
[28] V. I. Anisimov, J. Zaanen, O. K. Andersen, Band theory and Mott insulators: Hubbard *U* instead of Stoner *I*, Phys. Rev. B 44 (1991) 943.
[29] A. I. Liechtenstein, V. I. Anisimov, J. Zaanen, Density-functional theory and strong interactions: Orbital ordering in Mott-Hubbard insulators, Phys. Rev. B 52 (1995) R5467.
[30] J. P. Perdew, K. Burke, M. Ernzerhof, Generalized Gradient Approximation Made Simple, Phys. Rev. Lett. 77 (1996) 3865; Phys. Rev. Lett. 78 (1997) 1396.
[31] Bi -C. Shih, Y. Zhang, W. Zhang, and P. Zhang, Screened Coulomb interaction of localized electrons in solids from first principles, Phys. Rev. B 85 (2012) 045132.
[32] J. Heyd and G. E. Scuseria, J. Chem. Phys. 121 (2004) 1187.
[33] J. Klimeš, D. R. Bowler, and A. Michaelides, Chemical accuracy for the van der Waals density functional, J. Phys.: Cond. Matt. 22 (2010) 022201.
[34] J. Klimeš, D. R. Bowler, and A. Michaelides, Van der Waals density functionals applied to solids, Phys. Rev. B 83 (2011) 195131.
[35] H. D. Monkhorst, and J. D. Pack, Special points for brillonin-zone integrations, Phys. Rev. B 13 (1976) 5188.
[36] Crystal structure plots were made using VESTA. See K. Momma and F. Izumi, VESTA 3 for three-dimensional visualization of crystal, volumetric and morphology data, J. Appl. Crystallogr. 44 (2011) 1272. For other plots we used gnuplot (gnuplot.sourceforge.net), unless othwerwise specified.
[37] For the atomic positions in this slab, as well as in the slabs studied further on, please see Supplementary Material.
[38] N. Vorobyeva, M. Rumyantseva, D. Filatova, F. Spiridonov, V. Zaytsev, A. Zaytseva, and A. Gaskov, Highly Sensitive ZnO(Ga, In) for Sub-ppm Level NO_2 Detection: Effect of Indium Content, Chemosensors 5 (2017) 18.
[39] C. Freysoldt, B. Grabowski, T. Hickel, J. Neugebauer, G. Kresse, A. Janotti, and C. G. Van de Walle, First-principles calculations for point defects in solids, Rev. Mod. Phys. 86 (2014) 253.
[40] Note that in this work we consider only dopants in the neutral state, so there is no charge transfer to/from the Fermi sea. Thus, the corresponding term is absent from Eq. (2).
[41] W. Tang, E. Sanville, and G. Henkelman, A grid-based Bader analysis algorithm without lattice bias, J. Phys.: Condens. Matter 21 (2009) 084204.
[42] E. Sanville, S. D. Kenny, R. Smith, and G. Henkelman, Improved grid-based algorithm for Bader charge allocation, J. Comput. Chem. 28 (2007) 899.
[43] N. Barsan and U. Weimar, Conduction model of metal oxide gas sensors, J. Electroceram. 7 (2001) 143.
[44] W. Zeng, Y. Li, B. Miao, L. Lin, and Z. Wang, Recognition of carbon monoxide with SnO2/Ti thick-film sensor andits gas-sensing mechanism, Sensor. Actuat. B-Chem. 191 (2014) 1.
[45] R. Dhahri, M. Hjiri, L. El Mir, H. Alamri, A. Bonavita, D. Iannazzo, S. G. Leonardi, and G. Neri, CO sensing characteristics of In-doped ZnO semiconductor nanoparticles, J. Science: Adv. Mater. Devices 2 (2017) 34.
[46] R. R. Gay, M. H. Nodine, V. E. Henrich, H. J. Zeiger, and E. I. Solomon, Photoelectron study of the interaction of carbon monoxide with zinc oxide, J. Am. Chem. Soc. 102 (1980) 6752.
[47] F. Viñes, A. Iglesias-Juez, F. Illas, and M. Fernández-García, Hydroxyl Identification on ZnO by Infrared Spectroscopies: Theory and Experiments, J. Phys. Chem. C 118 (2014) 1492.
[48] The band structure plots were made using MATLAB (MATLAB 2018a, The MathWorks, Inc., Natick, Massachusetts, United States).
[49] R. Saniz, Y. Xu, M. Matsubara, M. N. Amini, H. Dixit, D. Lamoen, and B. Partoens, A simplified approach to the band gap correction of defect formation energies: Al, Ga, and In-doped ZnO, J. Phys. Chem. Solids 74 (2013) 45.
[50] A. Janotti and C. G. Van de Walle, LDA+U and hybrid functional calculations for defects in ZnO, SnO2, and TiO2, Phys. Status Solidi B 248 (2011) 799.